Numerical Methods in Civil Engineering

Evaluation of Wind Effects on Super-Tall Buildings using CFD Simulation and 3D Visualization

Freydoon Rezaie*, and Sayed Youness Hossieny Akhgar **

ARTICLE INFO

Article history:
Received:
August 2018.
Revised:
November 2018.
Accepted:
December 2018.

Keywords:
Wind
Computational
Fluid dynamics
High - rise building
Wind tunnel

Abstract:

In super-tall buildings, the impacts of wind loads are of more importance than earthquakes, and inevitably, the wind tunnel testing provides reliable results of the wind loads due to their high level of sensitivity and accuracy, although it burdens a high cost. In this paper, we have applied the 'numerical methods' in order to obtain the 2D and 3D drag coefficients. The CFD simulation was performed by the "ANSYS FLUENT" software. The results shown by the k-ω Shear Stress Transport (SST) turbulence model within a fine mesh and by selection of the small time-step size and also increasing the number of iterations… , prove that the accuracy of the analysis is enhanced in which it is valid for the Large Eddy Simulation (LES) model as well. The Grid Convergence Index (GCI) is obtained using the uniform velocity and pressure coefficients within a reasonable range, which is maintained by an average mesh in order to minimize the spent time and the associated cost. Meanwhile, the pressure-correction gradient along the cell faces is more compatible with the results obtained by Kawamoto except one point. As the duration of winding increases, the negative (vacuum) pressure on the leeward side develops and the wake also moves farther. The results also show that the maximum wind pressure applied to the building using the SST method is larger than the one in the LES method, but the LES method has less variation in height. Moreover, the wind resisting behavior of super tall buildings is better represented by3D modeling and the results of the simulation are more accurate and realistic, according to the experimental results.

1. Introduction

With the availability of powerful computers, the application of numerical methods to solve scientific and engineering problems is becoming a normal practice in engineering and scientific communities. Well-formed scientific theory with numerical methods may be used to study the scientific and engineering problems. The numerical methods flourish where an experimental work is limited, but it might be imprudent to view a numerical method as a substitute for experimental work(s). The growth in computer technology has made it possible to consider the application of partial deferential equations in science and engineering on a larger scale than ever. When experimental work's cost is prohibitive, a well-formed theory associated with numerical methods may be used to Obtain highly valuable information [1].

**Associate Professor, Faculty of Engineering, Bu-Ali Sinai University of Hamedan.*

***corresponding author: Msc Omran-Tosseeh, college of Engineering, Hamedan. Email: yakhgar57@gmail.com*

The fast-growing computational capacity also makes it practical to use numerical methods in order to solve problems. It is a common encounter that the Finite Difference (FD) or Finite Element (FE) numerical-methods-based applications are used to solve or simulate complex scientific and engineering problems [1]. Therefore, the Computational Fluid Dynamics (CFD) has emerged as a feasible solution in terms of both cost and accuracy, but it still needs some further improvements in order to be able to completely replace it with the wind tunnel testing [2]. Basically, there are two types of parameters that act as sources of error(s) in CFD analysis. First, there are modeling errors that arise from the applied turbulence modeling and the physical boundary conditions. The other errors stem from the numerical approximations. Existingly, the grid design, the truncation error of the discretization scheme and the error from incomplete iterative convergence influence on the final solution. There are several comparative studies that have been conducted in the last years assessing the influence of different parameters on the solution [3]. The application

of CFD in the wind engineering, called Computational Wind Engineering (CWE), has significantly ~~i~~ increased in the last two decades. Despite its widespread use, the general appraisal of the approach for the quantitative and sometimes qualitative predictions is expressed as lack of confidence, the main objection being the availability of many physical and numerical parameters used in the approach, which can be freely chosen by the user [4 - 8].

Murkami, 1990 [9] has provided some important points about the numerical simulation of turbulent air flow in the wind engineering. He has emphasized the need for the use of Navier-Stokes equations in the wind engineering, which generally includes the flow with a high Reynolds number. In this regard, different equations of turbulence are based on time averaging Reynolds Averaged Navier-Stokes (RANS) and the using LES has been reviewed and presented **.**A numerical study on the effect of wind on high-rise buildings with CAARC standard (Common wealth of Aviation Advisory Council) was conducted by Huang et al., 2007 [10].

Despite the rapid developments in computer technology, modern day computers are nowhere near to solving Direct Numerical Simulations (DNS) of the scale of prototype buildings. Therefore, as an alternative measure, the wind engineering research community has considered the use of time-averaging techniques and thereby solving the (RANS) equation only in the spatial domain, instead of the original Navier-Stokes Equation which spans over both spatial and time domains. The averaging process gives rise to an additional stress component termed as the Reynolds stress which is solved using turbulence modeling. Various turbulence models have been developed to accommodate different flow conditions [2]. The shear-stress transport (SST) κ-ω model was developed by Menter, 1994 [11]

The first use of CFD for indoor building airflow analysis was presented by Nielsen, 1973 [12]. Blocken, 2018 [13] cites Yamada and Meroney, 1971 [14] as doing the first work related to simulation of airflow around buildings.

In the past, especially the deficiencies of the steady RANS approach with the standard κ-ε model by Jones and Launder 1972 [15] for wind flow around buildings were addressed [16]. However, the main limitation of the steady RANS modelling remained its incapability to model the inherently transient features of the flow field such as the separation and recirculation downstream of windward edges and vortex shedding in the wake. These large-scale features can be explicitly resolved by the LES [16].

The primary concern for a structural engineer when studying the wind phenomena~~,~~ around a building, is the "mean velocity profile" of the wind stream. Moreover, two aspects of turbulent flows are of interest to the engineers: (a) the state of turbulence of the natural wind approaching a structure, and (b) the local turbulence in the wind by the structure itself. Most structures in the civil engineering present the bluff forms, and in the wind engineering studies we focus on the bluff-body aerodynamics aspects of the wind and structure interactions. This has led the industry to further research on the details of flow effects around the bluff bodies such as tall buildings. This finally leads to the interest of the engineer in the study of the development of body pressures by the flow acting around a structure [16].
In this paper, the influence of the time and repetitive parameters on coefficients in the SST and LES models ~~is~~ are investigated Next, the convergence of the three mesh types for the use of coarse or medium mesh rather than the fine mesh is studied (the medium one in this article). Eventually, the medium sized mesh is used to evaluate the wind pressure against the super tall buildings using the SST and LES methods.

2. Material and Methods

2.1 Governing equations in a turbulent flow

Most CFD software products solve a set of equations known as the Navier-Stokes (N-S) equations. These equations are based on the two conservation laws: (a) the conservation of mass and, (b) the conservation of momentum, whereas $u_i{}'$ denotes the fluctuating velocity. μ and ρ are the dynamic viscosity and specific mass of the fluid, respectively. The continuity equation for the compressible flow is:

$$\frac{\partial}{\partial x_i}(\overline{\rho\, u_\iota}) + \frac{\partial}{\partial x_i}(\overline{\rho'\, u_\iota{}'}) = 0 \tag{1}$$

For the incompressible flow:

$$\frac{\partial \bar{u}_i}{\partial x_i} = 0 \tag{2}$$

The momentum equation is:

$$\rho\left[\frac{\partial \bar{u}_i}{\partial t} + \bar{u}_j\frac{\partial \bar{u}_i}{\partial x_j}\right] = \bar{B}_\iota - \frac{\partial \bar{p}}{\partial x_i} + \frac{\partial}{\partial x_j}\left[\mu\frac{\partial \bar{u}_i}{\partial t} - \rho\overline{u_i' u_j'}\right] \tag{3}$$

The only difference between above momentum equations with the instantaneous quantity is $\rho\overline{u_i' u_j'}$. This term is called the Reynolds stress.

2.2 The Basic Relations in Eddy Viscosity

As stated above, the basic relations governing the eddy viscosity using a single parameter, the so-called turbulent viscosity μ_t, to express the relationship between the Reynolds stresses in the Rens equations and the profiles in the medium flow field. Three of these relationships are Bozynsk, Spziella and Lander, whose Bozynsk relationships is a permanent and basic relationship in the concept of Eddy viscosity [17]. The Bozynsk relationship is based on this principle that the components of the Reynolds stress are proportional to the average velocity gradients:

$$-\rho\overline{u_i'u_j'} = 2\mu_t S_{ij} - \frac{2}{3}\rho k\delta_{ij} \quad (4)$$

In which S_{ij} is the tensor of the strain rate, and above relation is incommensurable form of the Bozynsk equation, but the complete form of this equation, which includes the effects of the condensation of the current, is as follows:

$$-\rho\overline{u_i'u_j'} = 2\mu_i S_{ij} - \frac{2}{3}\delta_{ij}\frac{\partial u_k}{\partial x_k} - \frac{2}{3}\rho k\delta_{ij} \quad (5)$$

In the high Reynolds numbers, and in all or a significant portion of the current $\mu_t >> \mu$, the overall viscosity is written as follows:

$$\mu = \mu_0 + \mu_t \quad (6)$$

where μ is the viscosity of the flow and the fluid property), The RANS equations (with Reynolds stresses) can be eliminated by removing the Reynolds stresses and replacing the viscosity μ with viscosity equivalent to turbulent flows, the above relation can be similar to Navier-Stokes equations written as smooth currents that do not include the turbulent Reynolds tensor $\rho\overline{u_i'u_j'}$. Using this method, we can only look for a μ_t distribution in order to model a turbulent stream instead of a direct prediction of the value $S_{ij} = \left(\frac{u_{i,j}+u_{j,i}}{2}\right)$ [17].

2.3 Eddy viscosity models

The purpose of the eddy viscosity models is to describe the relationship between μ_t and physically measurable flow quantities or calculated field flow quantities. In general, these models can be divided into three categories [17]. Equivalent zero models use only algebraic relations and equations to describe the relationship between μ_t and calculated or measurable properties. Models of an equation of Spalart-Allmaras:

$$-\rho\overline{u_i'u_j'} = 2\mu_t S_{ij} - \frac{2}{3}\delta_{ij}\frac{\partial u_k}{\partial x_k} - \frac{2}{3}\rho k\delta_{ij} \quad (7)$$

The last sentence is deleted because of the absence of *k* [18]. Two-equation models include the two extra equations like SST and LES methods which have been the basis for a high number of researches. Obviously, there is no any disturbance model(s) that is responsive to the all engineering issues. The 2003 SST model's transport equations are given by Menter et al., 2003 [19].

$$\frac{D(\rho k)}{Dt} = \widetilde{P_K} - \beta^*\rho k\omega + \nabla.[(\mu + \sigma_k\mu_t)\nabla k] \quad (8)$$

$$\frac{D(\rho k)}{Dt} = \frac{v}{v_t}\widetilde{P_K} - \beta\rho\omega^2 + \nabla.[(\mu + \sigma_\omega\mu_t)\nabla\omega] + 2\,(1 - F1)\,\rho\sigma_{\omega 2}\frac{1}{\omega}\nabla k \cdot \nabla\omega \quad (9)$$

Where the eddy viscosity (kinematic) is:

$$v_t = \frac{\mu_t}{\rho} = \frac{a_1 K}{max\{a1\omega, SF2\}} \quad (10)$$

$$\hat{v}_t = max\{v_t, 10^{-8}\} \quad (11)$$

And the production terms are:

$$P_K = (2\mu_t S_{ij} - \frac{2}{3}\delta_{ij}\frac{\partial u_k}{\partial x_k} - \frac{2}{3}\rho k\delta_{ij})U_{i,j} \quad (12)$$

$$P_k = min\{P_k, 10\beta^*\rho k\omega\} \quad (13)$$

The functions F_1 and F_2 (Equations 13 and 14) use wall distance to blend the near-wall k-ω model with the away-from-wall k-ε closure (recast into k-ω variables), this being a fundamental attribute of the SST model.

$$F_1 = tanh\ ([max\{2.5, \frac{61.5}{y+}\}]^4 \quad (14)$$

$$F_2 = tanh\ ([max\{1.35, \frac{61.5}{y+}\}]^2 \quad (15)$$

Note that this is strictly a limited representation of the blending functions in the logarithmic region and not a general indication that they can be expressed in terms of $y+$. Equation 13 indicates that $F_1=1$, hence the *k-ω* constants will be used in the logarithmic overlap region. From Equation 14, $1 \geq F_2 \geq 0.95$, which retains the basic SST like eddy viscosity formula. In the original SST closure $F_1=F_2=1$ in the viscous sub layer and the logarithmic overlap, diminishing toward *Zero* in the defect layer (a wall distance) [20]. As mentioned The SST *κ-ω* model is equivalent to the standard model, but it includes the following refinements:

1. The standard *κ-ω* and the transformed *κ-ε* models are multiplied by a blending function and then they are summed together. The function is designed to have a value of one in the near wall region, and zero away from the surface.
2. The SST model includes a damped cross-diffusion derivative term in the ω equation.
3. The definition of the turbulent viscosity is modified to account for the transport of shear stress.
4. The constants in these models have different values.

The major way in which the shear-stress transport (SST) model differs from the standard model.

$$\frac{\partial(\rho k)}{\partial t} + \frac{\partial(\rho k u_i)}{\partial x_i} = \frac{\partial}{\partial x_j}\left[\left(\mu + \frac{\mu_t}{\sigma_k}\right)\frac{\partial k}{\partial x_j}\right] + G_K + G_b - \rho\varepsilon - Y_M + S_k \quad (16)$$

$$\frac{\partial(\rho\varepsilon)}{\partial t} + \frac{\partial(\rho\varepsilon u_i)}{\partial x_i} = \frac{\partial}{\partial x_j}\left[\left(\mu + \frac{\mu_t}{\sigma_\varepsilon}\right)\frac{\partial\varepsilon}{\partial x_j}\right] + C_{1\varepsilon}\frac{\varepsilon}{k}(G_K + C_{3\varepsilon}G_b) - C_{2\varepsilon}\rho\frac{\varepsilon^2}{k} + S_\varepsilon \quad (17)$$

In the above equations, $G\kappa$, represents the generation of turbulence kinetic energy due to mean velocity gradients. $G\omega$ represents the generation of ω. $\Gamma\kappa$ and $\Gamma\omega$ represent the effective diffusivity of κ and ω, respectively. Yk represents the dissipation of κ and $Y\omega$ the dissipation of ω due to turbulence. $D\omega$ represents the cross-diffusion term. These terms have specific models associated with them that are left to the reader to reference to lastly, $S\kappa$ and $S\omega$ are user defined source terms [21].

A different approach to the computation of turbulent flows accepts that the larger eddies need to be computed for each problem with a time-dependent simulation. The universal behavior of the smaller eddies should be easier to capture with a compact model. Instead of time-averaging, the LES uses spatial filtering to separate the larger from smaller eddies. This method uses the selection of a filtering function and a certain cutoff length scale with the aim of resolving in an unsteady flow computation all those eddies that have a larger length scale than the cutoff dimension. During the spatial filtering, the information related to the smaller eddies below the cutoff length is destroyed. This interaction effects between larger and smaller eddies give rise to Sub-Grid-Scale (SGS) stresses. This is the key concept of the large eddy simulation (LES) approach to the numerical treatment and solution of turbulence in fluids.

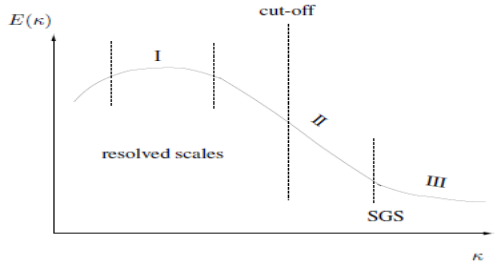

Fig. 1: Spectrum of velocity [12]

The rationale behind LES can be interpreted as: (1) momentum, mass, energy and other scalars are transported by larger eddies, (2) larger eddies are highly problem-dependent; as they are governed by the geometry and boundary conditions of the flow, (3) smaller eddies do not depend on geometry, and they are isotropic. By resolving the large eddies the must use finer meshes than those used in the RANS models. The LES has to be typically run for long duration of time to obtain stable statistics for the flow being modeled [21].

2.4 Near Wall Treatment (Approach)

It is critical to capture boundary layer near wall properly. In order to do that, the mesh should be generated in such a manner that it captures the boundary layer properly. For turbulent flows, calculation of the y+ value of the first interior grid point helps achieve the capture of the boundary layer [16].

In this simulation, a very fine grid cell model is used near the wall region and y+ is less than 5 (preferably 1) to fit well into the inner layer. The method is to use the following relationships to obtain the first mesh distance from the wall.

$$C_f = \frac{0.026}{Re_x^{\frac{1}{7}}} \tag{18}$$

$$\tau_{wall} = \frac{C_f \rho U_\infty{}^2}{2} \tag{19}$$

$$U_{fric} = \sqrt{\frac{\tau_{wall}}{\rho}} \tag{20}$$

$$\Delta s = \frac{\mu y +}{U_{fric}\rho} \tag{21}$$

$\mathbf{C_f}$ is friction factor, $\boldsymbol{\tau_{wall}}$ is shear stress, $\mathbf{\Delta s}$ is distance of first mesh and $\mathbf{U_{fric}}$ is friction velocity.

2.5 Simulation Method with Ansys Fluent Software

A numerical simulation is a mathematical recreation of a natural process. By using numerical simulations, it is possible to study physical processes. Thus, the field of numerical simulations represents a rich field of interdisciplinary research. Some of the scientific problems are studied principally through the use of numerical simulations, such as those scientific fields that are governed by non-linear simultaneous equations, or those that are not easily reproducible in the laboratory. The use of these to study a problem normally requires a careful study of the numerical methods and algorithms that will be used and the fundamental process that will be included. A numerical simulation differs from a mathematical model in the sense that the first one is a representation in every instant of the process that will be simulated, while the second one is a mathematical abstraction of the fundamental equations necessary to analyze the phenomenon. Normally, the use of a numerical simulation in the analysis of a given problem requires a careful planning of the mathematical model that will be used and the necessary algorithms that will be employed [1].

Similar to other numerical methods developed for the simulation of fluid flow, the finite volume method transforms the set of partial differential equations into a system of linear algebraic equations. Nevertheless, the discretization procedure used in the finite volume method is distinctive and involves two basic steps. In the first step, the partial differential equations are integrated and transformed into balance equations over an element. This involves changing the surface and volume integrals into discrete algebraic relations over elements and their surfaces using an integration quadrature of a specified order of accuracy. In the second step, interpolation profiles are chosen to approximate the variation of the variables with in the

element and relate the surface values of the variables to their values and thus form the algebraic relations into algebraic equations [22].

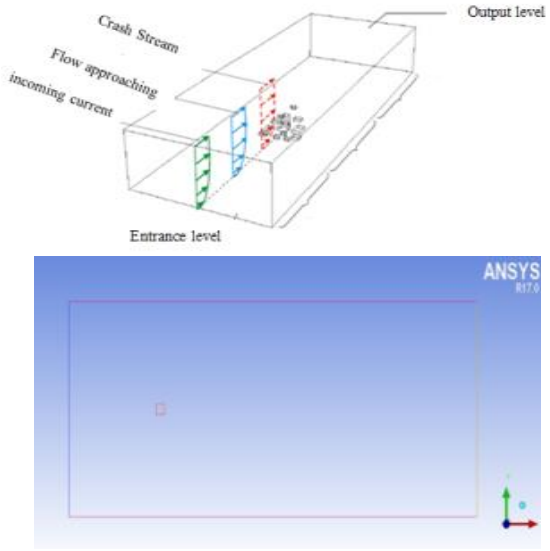

Fig. 2a: Computational Domain Display **2b:** Computational Domain Model

The size of the computing domain has no relationship. Usually this size is calculated based on the geometry of the building and is a multiple of the building's dimension or height. This size is calculated based on the upstream or downstream flow. For the model presented in this paper, (Fig. 2b), the prototype is a 40-meter-square, 40-meter-wide, 300-meter-high square building. The wind tunnel scale 1: 400 is selected and its dimensions reduced to 0.1 × 0.1 × 0.75 meters.

In this article, three types of meshing are used, respectively coarse, average and fine. The ANSYS ICEM is used for 2D geometry. in fine meshing 157000 node is used and in large meshing this amount becomes 1/2 and in large meshing 1/4. The distance between the first mesh of the obstacle is same in all three models.

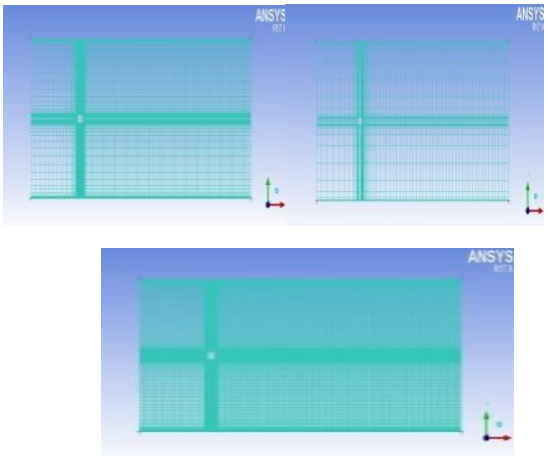

Fig. 3: three meshing fine- medium-Coarse

In the table below boundary condition that used in this research is shown.

Table. 1: Model boundary condition (SST)

μ $(^{kg.s}/_{m^2})$	ρ $kg.s/m^2$	(m/s) V_{10}	p (pa)	T (k)	Much. n
0.000018375	1.255	21.53	101325	300	0.5

Table. 2: Reduce dimension (Similarity model and sample)

quantity	length	time	velocity
scale	1/400	1/100	1/4

V_{10} is velocity of wind (or hurricane) in 10 meter above of earth

Table. 3: Δs distance of first mesh

Re	C_f	$\tau_{w\rho all}$ (Pa)	U_{fric} (m/s)	Δs (m)
233333.33	0.0044	3.40	1.6	0.000009

Furthermore, similarity condition between sample and model is mentioned. Also, in the present study the SST and LES are utilized for the modeling of the wind flow around the bluff body. In principle, the Reynolds number ratio must be the same for the similarity between the sample and the wind tunnel. In the wind tunnel, of course, the fluid used is atmospheric pressure and the Reynolds number similarity is violated.

3. Results and Discussions

3.1 Time and iterative effects in evaluation of C_d and C_f (2D)

The drag coefficient is a function of dimensional parameters such as Reynolds number, Mach number, Froude number, and relative roughness. A square cylinder has been found out to be a C_d value of approximately 2.10 derived from experimental studies as reported in Table 8 [16].

Table. 4: Experimental data and derived quantities for various cross sections [16]

Source	*Re*	c_D	*St*
Store belt bridge	2×10^6	0.600	0.220
Store belt bridge	50 000	0.680	0.180
Circular cylinder	4500	0.700	0.217
Tacoma bridge	6×10^5	1.25	0.117
Square cylinder	1.76×10^5	2.04	0.122
Square cylinder	10^5	2.05	0.118
Square cylinder	13 000	0.216	0.132
Inclined square cylinder	6×10^5	2.40	0.120

The drag and lift force obtained from the CFD for fine mesh are shown in Fig. 4.

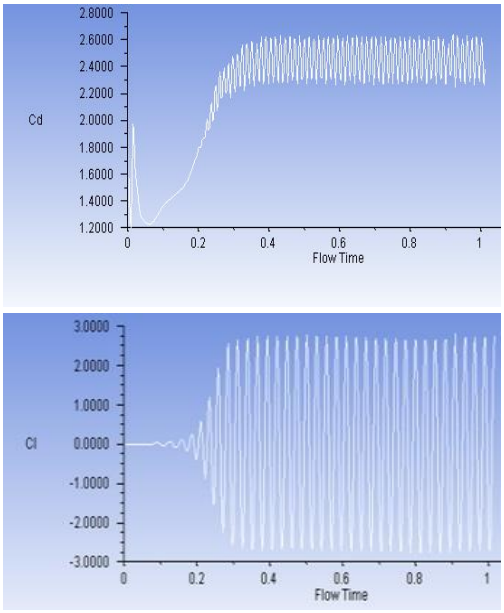

Fig. 4: Drag and Lift coefficient in fine mesh

For validation of the model and considering the turbulent fluid behavior, the C_d is determined and compared with the data given in the Table 4. According to it (wind tunnel results) and linear extrapolation, for example it is seen that C_d for the cross section is *2.037*. The results obtained by simulation are also compared with them. Of course, as shown below, in the medium mesh, the range is closer to the exact answer. Also, the results of the simulation with a time interval of 0.003 sec with effect time 1 sec for the three types of meshing are shown in the following Table 5.

Reynolds = 2.396×10^5 Iterative= 40

Table. 5: Comparison simulation results for a height of 300 m in three meshing (SST)

mesh	C_d	C_l
Fine	2.15 - 2.35	2.15
Medium	1.95 - 2.15	1.9
Coarse	1.65 - 1.75	0.95

Also, for iterative=40 in fine mesh for difference time step these coefficients obtained (two convergence scale). The Table below shows that the smaller the time step, the coefficients get closer to the actual value but calculation time increase.

Table. 6: Results of fine mesh simulation with different time steps of convergence are scaled $\times 10^{-5}$

Time Step	C_d	C_l
0.003	2.15-2.35	2.15
0.001	2.02-2.62	2.5
0.0001	1.94-2.26	2.21

Table. 7: Results of fine mesh simulation with different time steps of convergence are scaled $\times 10^{-3}$

Time step	C_d	C_l
0.003	2.30-2.70	2.75
0.00235	2.25-2.75	1.75
0.00134	2.15-3.00	1.75
0.000134	1.95-2.70	2.50
0.0000134	1.90-2.4	2.45

3.2 Time and iterative effects in evaluation of C_d and C_f (3D)

LES model is used to separate large vortices from small, as you know larger vortices contain kinetic energy and the mesh must be positioned to accommodate the larger vortex. In this paper, the irregular geometrical modeling is used. As seen in Table 8, the model has been analyzed by two piezo and couple methods in different periods of time. In piezo mode once the time step 0.003 and the other load of 0.0002 has considered.

Table. 8: Boundary conditions and values of C_d in 3D model

Iterative	Time step	Time effect	method	C_d
8376	0.003	0.639	piezo	0.84553
8420	0.003	0.630	couple	0.846
20176	0.0002	0.1	piezo	0.868

According to Fig. 5, the oscillatory behavior of the coefficients is higher in the couple method and thus ~~is~~ it has used the piezo method. Importantly, the drag coefficient for the rectangular cube is about 1.05 (Valid sources). Table 8 shows that the smaller the time step chosen, the closer the answer is to the exact number. Also, this small time step can converge faster in less effect time.

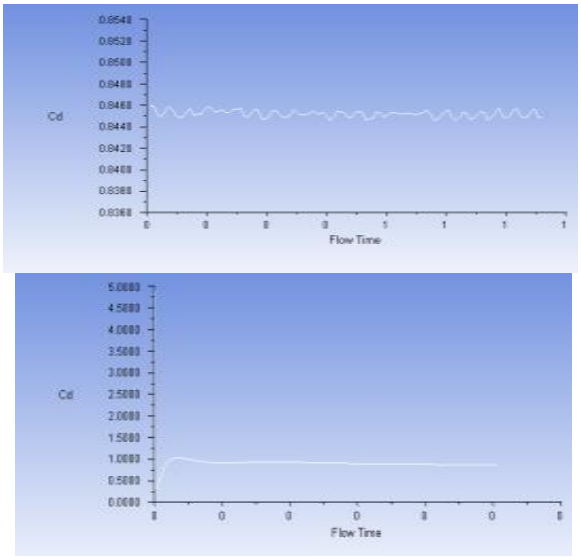

Fig. 5: Display of C_d in Couple (top) and Piezo methods

3.3 The study of Grid Independence

A grid sensitivity analysis for the model was performed using different number of nodes in increasing multiples of two. This type of analysis must be performed to reduce the influence of the number of nodes on the computational results since the solution must be independent of the mesh resolution in the computational domain. It is good practice to run this study before a more global analysis of the system is completed [16]. As it is mentioned in the case of our model, the prototype is a square structure dimensioned as 40 meter (length) by 40 meter (Width) in plan form, and height is 300 meter (H) in order for it to qualify as a super-tall building.

The GCI method (which is based on RE) described herein is an acceptable and recommended method that has been evaluated over several hundred CFD cases [23, 24, 25, 26, 27, 28]. The Grid Convergence Index (GCI) provides a uniform measure of convergence for grid refinement studies by Roche. It is based on estimated fractional error derived from the generalization of Richardson extrapolation. The GCI value represents the resolution level and how much the solution approaches the asymptotic value [29].

The GCI can be written as;

$$GCI_{21=}F_S\frac{|\varepsilon_{21}|}{f_1(r^p-1)}<5 \qquad (22)$$

$$\mathrm{GCI}_{32=}F_S\frac{|\varepsilon_{32}|}{f_2(r^p-1)}<5 \qquad (23)$$

The grid independent study was validated using two different data outputs from the model [16]. The first data is chosen in this research to ensure that the grid convergence is the velocity convergence.

Table. 9: boundary condition for three meshing

X(m)	f_1(m/s)	f_2(m/s)	f_3(m/s)
0.554	0.87178	0.87266	0.87913

Table. 10: GCI of velocity for 3 meshing

ε_{21}	0.00088	**p**	2.8772
ε_{32}	0.00647	**lnr**	0.6931
$\mathbf{GCI_{21}}$	1.986×10^-4		
$\mathbf{GCI_{32}}$	1.459×10^-4		

For such high quality studies a Modest and more palatable value of Fs=1.25 appart to be adequately conservative. However, for the more Common two grid study (often performe reluctatly, at the insistance of journal editors) I still recommend the value Fs=3 for the sake of uniform reporting and adequate conservatism [30]. In this research Fs= 1.25.

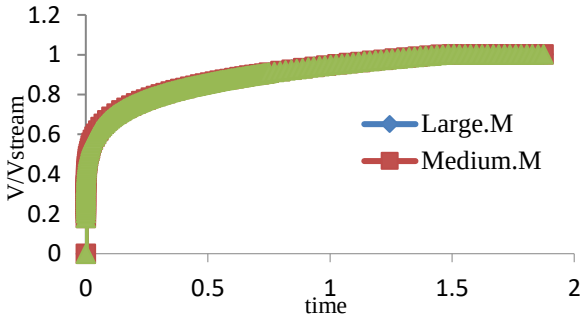

Fig. 6: normalize velocity from south wall

The second data is chosen in this research to ensure of the grid convergence is the pressure coefficient (Cp), as presented in Fig. 7. The effects of the wind on a building are usually determined using the external pressure coefficient Cpe [18]. The pressure coefficient describes the relative pressure throughout a flow field in fluid dynamics and it is a dimensionless number. In engineering modeling of fluid dynamics problems, this number is of paramount importance since a model can be tested at a wind tunnel scale where the values can be determined at critical locations, and these same coefficients can be used with confidence to predict the fluid pressure at these same critical locations of the full-scale structure [16].

Table. 11: boundary condition for three meshing

X(m)	f_1(m/s)	f_2(m/s)	f_3(m/s)
1.05	1.2160	1.2031	1.1574

Table. 12: GCI of pressure coefficient for three meshing

ε_{21}	0.0129	**p**	1.825
ε_{32}	0.0457	**lnr**	.6931
GCI_{21}	0.5		
GCI_{32}	1.87		

Comparison of mean Cp values at $y / B = 0.5$ for three cases with time step= 0.67 shown in Fig. 5. y / B is the ratio of the position of the point to the width of the model because the wind pressure is higher in the middle of the windward face, so in the SST this ratio is assumed to be 0.5, i.e. $y / B = 0.5$.

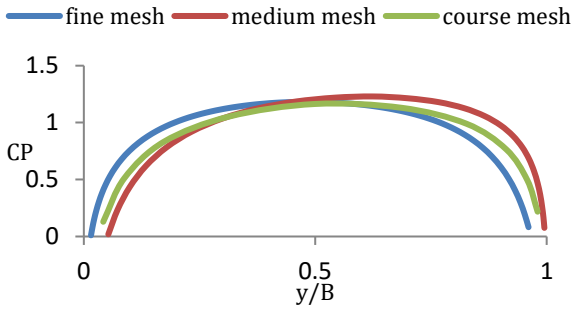

Fig. 7: Variation of mean pressure coefficient along the WindWard face for grid analysis

3.4 Evaluation of mean pressure coefficient along faces of a square prism

A property has been compared to previous experimental studies and CFD analysis performed by Kawamoto in which the pressure coefficients were measured along the four faces of a square prism.

Comparison of the coefficients obtained with Fig. 8 shows that in the windward, the sideward and the leeward are in good agreement with the coefficients of the previous researchers and all three times overlap, but in the sideward 3-4 and near the edge 3 shift in the direction of the pressure coefficient is observed.

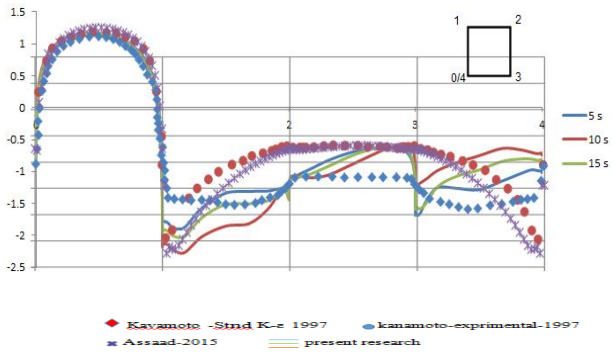

Fig. 8: Variation of mean pressure coefficient along face

However, the results of this article are more consistent with Kawamoto-Experimental's results in same face, except for point 3 that results are different. Another point is that the wind behavior for mean pressure coefficient along face in 5 sec is much closer to 15 sec.

3.5 Effect of the effective time of wind on pressure and velocity contours

Contours in ANSYS represent a region of pressure or velocity. Fig. 9 shows the pressure contours at a height of 300 meters (highest point of the building). In pressure the areas in red represent the maximum and the areas in blue represent the minimum.

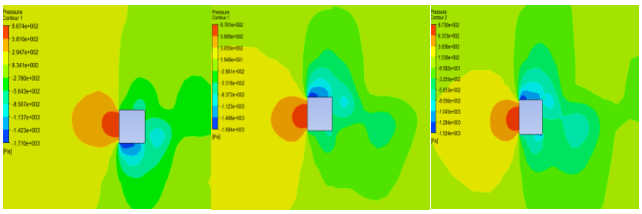

Fig. 9: Display pressure contours on both sides of the model 0.3 s **9b:** 3 s **9c:** 15 s (left to right)

In the windward, here is only positive pressure. The positive and negative pressure difference causes a dragged force that forces the region to exert negative pressure and cause the spiral movement to produce a vortex flow. According to Fig. 9, increase of time cause to decrease of positive pressure region in windward and increase negative pressure region in leeward.

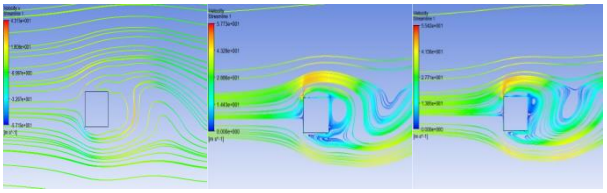

Fig. 10: Flow variation around building model with at various time lapse in 300 m

The above shapes represent the speed lines around the obstacle with 100 points in CFX. At 3 sec, the separation area is on the same edges of the building, and the eddy current corresponds to the leeward and top. At the influence time of the 15 second, the flow of external and internal lines increases and the number of lines with curvature of the velocity increases. In the vortex flow, the speed of the flow lines is reduced and the velocity goes to zero in the interior of the vortices. In other words, in the early time wake region is tangential to the leeward (in 3 s) and with the increase of the duration of the wind (to 15 s) the wake region will be further away from the building.

Also, the fluid outputs in Fig. 11 show the pressure lines. Higher values are highlighted in red and lower values are blue color. The pressure change along the sides of the LES model really reflects the wind behavior that operates on the body of the structure.

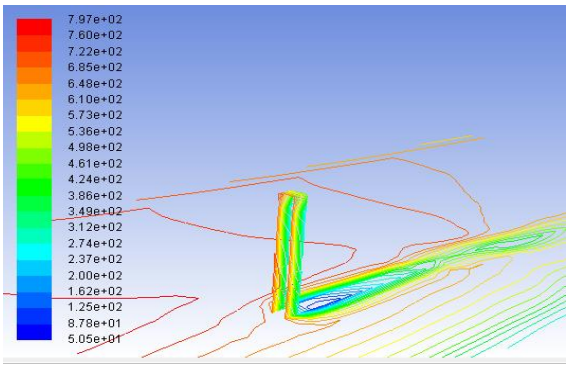

Fig. 11: Display Pressure contours along the height of the model

3.6 comparing the SST, LES methods

As previously mentioned, In Ansys contours represent a region of pressure or velocity, this paper attempts to represent the values of pressure at altitude as a unit value, this value being the maximum value of wind pressure at the same altitude (bottom figure) as used for simplification. However, this method is conservative.

The maximum pressure on the super tall building in this research (Fig. 12) is determined .In the SST method, it is clear that the maximum positive pressure in the center of the windward face that is drawn for different heights. The SST model this pressure is estimated about 1573 kg/m^2 which approximately 40% is larger than the LES model, this maximum for LES model is 1129 kg/m^2.

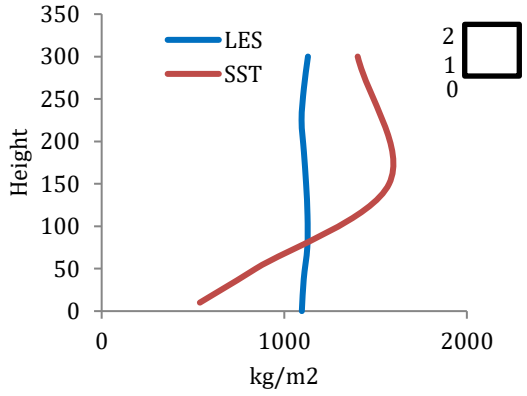

.

Fig. 12: Windward estimated pressure variation, SST, LES

Fig. 12 shows the pressure values per unit surface, which need to be multiplied the maximum values per height to convert the pressure values to the wind force, height values are assumed to be 4 meters (height of each building floor) , as well as the width of the building being 40 meters. The maximum force (Fig. 13), in the SST method, is estimated about 2493.5 kN which is larger than the LES maximum for LES model (1789.7 kN).

The SST overestimates the wind loads in the tall building model because it recognizes the maximum value at the center of the wind and simplifies the wind behavior, while the LES model shows the wind behavior more accurately.

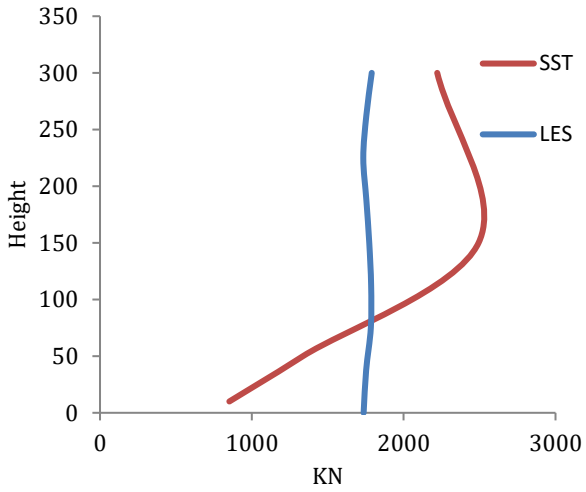

Fig. 13: Windward estimated force variation, SST, LES

4. Conclusions

The results show that in the 2D method, the Drag and Lift coefficients with small time step especially in fine mesh, errors between simulation answer and exact answer will be zero and increasing time and iterative of operation caused to increase accuracy. In the 3D method small time step help to exact answer. Convergence index, GCI, for three meshing is acceptable and thus coarse or medium mesh can use instead fine mesh (medium in this paper) to decrease time and cost. Mean pressure coefficient along faces of square has good agreement with the results of Kawamoto and Assad except for the 3-4 edges, although, Kawamoto's results Kawamoto–Stnd K-ε and Kawamoto-Experimental are not the same .The results of this paper show that the change is in line with the results of previous work in point 3. The results show that in the early stages of the wind effect, the maximum positive pressure is on the windward and the most negative pressure enters the side of the building, so wake occurs. Also, with increasing time of effect wind, the lines of the internal flow velocity of the vortex will be more curved, and the velocity of the vortex reaches zero.

Investigating different methods for determining the pressure on super tall buildings shows that the maximum pressure on the structure of the building using the 2D SST

method is larger than the LES model. The LES method has less variations in height than the SST method. The SST in medium class seemed to be conservative. So the more move to 3D modeling, which in turn requires faster computers, the modeling of wind behavior against super tall buildings improves and the simulation solutions become more accurate and could be close to laboratory results.

It can be mentioned that the numerical simulation by CFD can be used as an alternative to using wind pressure loading for a super tall building project at least before design. The results of this method should be carefully monitored and controlled. With suitable boundary conditions applied to the model and the development of computational resources, this method can be useful for wind load studies in the future.

References:

[1] Awrejcewicz, J., "Numerical analysis theory and application", 2011, ISBN 978-953-307-389-7

[2] Koliyabandara, S.M.N.H., Jayasundara, H.M.A.D., Wijesundara, K.K., "Evaluation of Different Turbulence Models in Determining Wind Loads on Tall Buildings", 2018.

[3] Casey, M., Wintergerste, T., "Quality and Trust in Industrial CFD", Best Practice Guidelines, editors, *ERCOFTAC SIG* ERCOFTAC, 2000.

[4] Franke, J., Hirsch, C., Jensen, A.G., Krüs. H.W., Schatzmann, M.,Westbury, P.S., Miles, S.D., Wisse, J.A., Wright, N.G., "Recommendations on the use of CFD in wind engineering", 2004.

[5] Castro, I.P., "CFD for external aerodynamics in the built environment", The QNET-CFD Network Newsletter, Vol. 2, 2003, 4-7.

[6] Schatzmann, M., Leitl, B., "Validation and application of obstacle-resolving urban dispersion models", Atmospheric Environment, Vol. 36, 2002, 4811-4821.

[7] Westbury, P.S., Miles, S., Stathopoulos, T., "CFD application on the evaluation of pedestrian-level winds", in G.Augusti, C. Borri, and C. Sacré, editors, Impact of Wind and Storm on City life and Built Environment, 2002, pages 172-181, CSTB, Nantes.

[8] Stathopoulos, T., "The numerical wind tunnel for industrial aerodynamics: Real or virtual in the new millenium?", Wind & Structures, Vol. 5, 2002, 193-208.

[9] Murakami, S., "Computational wind engineering", Journal of Wind Engineering and Industrial Aerodynamics, 1990, 36 (Part 1), 517-538.

[10] Huang, Sh., Li, QS., Xu, Sh., "Numerical evaluation of wind effects on a tall steel building by CFD", Journal of Constructional Steel Research, 2007, 63 (5), 612-627.

[11] Menter, F., "Two-equation Eddy-Viscosity Turbulence Model for Engineering Applications", AIAA, 1994, Vol. 32(8), 1598-1605.

[12] Nielsen, P., "Berechnung der Luftbewegung in Einem Zwangsbelufteten Raum", Gesundheits-Ingenieur, 1973, 299-302.

[13] Blocken, B., "LES over RANS in Building Simulation for Outdoor and Indoor Applications: A Foregone Conclusion?", Building Simulation, 2018, 821-870.

[14] Yamada, T., Meroney, R.N., "Numerical and Wind Tunnel Simulation of Airflow Over an Obstacle", In Proceedings of the National Conference on Atmospheric Waves, Salt Lake City: 1971.

[15] Jones, W., Launder, B., "The prediction of laminarization with a two-equation model of turbulence", Int. J. Heat Mass Transf, 1972, 301–314.

[16] Assaad, B., "Wind effect on super tall buildings using computational fluid dynamics and structural dynamics", thesis submitted to the faculty of the college of engineering and computer science, Florida Atlantic university, Boca Raton, 2015, 124 pages.

[17] Saebi, H., "Numerical analysis of two-dimensional incompressible fluid flow on a simple finite element method by finite element method", Islamic Azad University of Mashhad, MSc in Mechanical Engineering Eenergy Transformation Tendency Faculty of Engineering, 2013.

[18] Nasa space place, "How do hurricanes form?", https:// spaceplace.nasa.gov/ hurricanes/en, 2016.

[19] Menter, F.R., Kuntz, M., Langtry, R., "Turbulence, heat and mass transfer", 2003, pp. 625–632.

[20] Goldberg, U., Batten, P.,"wall-distance-free version of the SST turbulence model", Engineering Applications of Computational Fluid Mechanics, Vol. 9, 2015, 33–40.

[21] ANSYS, Inc, 2014, Fluent – Theory Guide, Canonsburg, PA.

[22] Moukalled, F., Mangani, L., Darwi, M., "Fluid mechanics and its applications", book series, FMIA, vol. 113, 2016.

[23] B. Celik, I, Ghia, U., J. Roache, P., Freitas, C., "Procedure for estimation and reporting of uncertainty due to discretization in CFD applications", mechanical and aerospace engineering department West Virginia university, Morgan town WV (USA), 2008.

[24] Roache, P.J., Ghia, K.N., White, F.M., "Editorial Policy Statement on Control of Numerical Accuracy", Journal of Fluids Engineering, 1986.

[25] Richardson, L.F., Gaunt, J. A., "The deferred approach to the Limit", philosophical transactions of the royal society of london, 1927, Series A, 226, pp. 299-361.

[26] Roache, P.J., "A method for uniform reporting of grid refinement studies", proceedings of quantification of uncertainty in computation fluid dynamics, 1993, 23-24.

[27] Eça, L., Hoekstra, M., Roache, P.J., "Verification of Calculations: an Overview of the lisbon workshop", AIAA Computational Fluid, Dynamics Conference, Toronto, 2005.

[28] Eça, L., Hoekstra, M., Roache P.J., "Verification of calculations: an overview of the 2nd lisbon workshop", AIAA Paper, 2007.

[29] Mat ALI, M.S., DOOLAN, C.J., Wheatley, V., "Grid convergence study for a two-dimensional simulation of flow around a square sylinder at a low Raynolds number", seventh international conference on CFD in the minerals and process industries CSIRO, Melbourne, Australia, 2009.

[30] Roache, P.J., "Quantification of uncertainty in computational fluid dynamics", Annu. Rev. Fluid. Mech, 1997, 123–60